

Cite this article as: Peng Jian, Tu Yi, Xue Zhichao, et al. Effects of Heat Treatment on Mechanical Property Distribution and Matching Degree of Welding Joint of Cr-Mo Steel Base Metal with Ni-based Welding Material[J]. Rare Metal Materials and Engineering, 2022, 51(11): 4059-4066.

ARTICLE

Effects of Heat Treatment on Mechanical Property Distribution and Matching Degree of Welding Joint of Cr-Mo Steel Base Metal with Ni-based Welding Material

Peng Jian, Tu Yi, Xue Zhichao, Miao Xinting, Liu Xuedong

School of Mechanical Engineering and Rail Transit, Changzhou University, Changzhou 213164, China

Abstract: Based on the advantages of digital image correlation method in the characterization of local mechanical property for welding joint, the differences in mechanical property, hardness, and microstructure of as-received, tempered, and solution treatment and aging (STA)-treated welding joints of 15CrMoR base metal with Ni-based welding material were compared. The tempering treatment transforms the dendritic structure into the dispersed tempered sorbite in the welding fusion zone (WFZ). The uniformity of mechanical properties is improved, and the matching degree of mechanical property between base metal zone (BMZ) and WFZ is improved. STA treatment transforms the dendritic structure into the uniform columnar dendrite structure in WFZ, which causes the disappearance of pearlite and the grain coarsening in BMZ, resulting in the degradation of strength and the increase of mismatching degree between WFZ and BMZ. Therefore, the suitable heat treatment needs to balance the requirements of BMZ and WFZ to obtain the excellent comprehensive mechanical property for welding joints.

Key words: Ni-based welding joint; heat treatment; digital image correlation; mechanical property distribution

Since the nickel-based welding material undergoes the deoxygenation and desulfurization in the welding metal melting pool, the weld porosity and crack are reduced. Besides the nickel-based materials^[1], the steel^[2,3] and titanium-zirconium-molybdenum alloy^[4] can also be welded through those treatments. Mittal et al^[5] used the nickel-based welding material in the welding of dissimilar T91/347H steels, and obtained higher tensile strength and better ductility of the welding part, compared with those of the austenitic welding materials. Kumar et al^[6] compared the tensile strength and fracture toughness of dissimilar joints of different ER309L/ER308L nickel-based welding materials with Inconel 82/Inconel alloys at different zones, including the heat affected zone (HAZ), welding fusion zone (WFZ), and base metal zone (BMZ). Awale et al^[7] studied the effect of heat treatment on the microstructure and tensile strength of P91/316LN dissimilar welding joints with the Inconel-182 welding material prepared by electrode arc welding. Wang et al^[8,9] studied the effects of different annealing treatments on the

microstructure and mechanical properties of Ni-based superalloy. Qi et al^[10] investigated the G115-deposited metal after different tempering treatments at 760, 800, and 820 °C, proved that the high temperature tempering treatment can eliminate the welding stress and structural stress, and obtained excellent comprehensive mechanical strength of welding parts. Xu et al^[11] studied the effect of three aging treatments on the Inconel 625 Ni-based superalloy prepared by pulsed plasma arc deposition. It is found that the direct aging, homogenized solution, and aging treatments cause the significant reduction of plasticity, whereas the solution treatment and aging (STA) treatment improves the mechanical strength without sacrificing the ductility.

The microstructure and mechanical strength of alloys have been widely studied, but the mechanical property distribution of different zones of welding joints is rarely reported. Wan et al^[12] investigated the variation in mechanical properties of different zones of the duplex stainless steel welding joint with the X-type weld groove by the micro-samples. The

Received date: December 06, 2021

Foundation item: National Natural Science Foundation of China (52075050, 52105141); Natural Science Foundation of Jiangsu Province (BK20201448)

Corresponding author: Peng Jian, Ph. D., Associate Professor, School of Mechanical Engineering and Rail Transit, Changzhou University, Changzhou 213164, P. R. China, E-mail: jpeng@cczu.edu.cn

Copyright © 2022, Northwest Institute for Nonferrous Metal Research. Published by Science Press. All rights reserved.

preparation of micro-sample is complex, and it is difficult to obtain the overall mechanical property distribution of the welding joint. The digital image correlation (DIC) method^[13,14] provides a feasible method to explore the distribution of mechanical property for the structure and material with local inhomogeneity. By analyzing the digital images during the deformation, DIC method provides the full-field displacement and strain distributions with sub-pixel accuracy, and can realize micro-scale and nano-scale deformation measurement^[15,16], therefore offering the local strain field distribution of the welding joint. Li et al^[17] obtained the strain hardening exponent on different zones of tailor-welded blanks by DIC method. By combining DIC method and inverse modeling technique, the strength coefficient can be determined for welding structure. Xie et al^[18] used DIC method to observe the deformation distribution of duplex stainless steel multi-pass weld joints during the monotonic tensile tests. The relatively homogeneous deformation distribution can be observed at elastic stage, but the deformation is concentrated at BMZ once the load exceeds the yield load during the hardening stage. Ren et al^[19] used DIC method to observe the strain distribution of steel plate weld joint and found that the high plastic strain accumulation in HAZ is responsible for the majority of failures in the welded joints, strongly influencing the fatigue behavior. DIC method can also be used to investigate the fatigue crack growth behavior^[20]. Furthermore, Sun et al^[21] used DIC method to study the full-field creep strain of the TA2 welded joint, and found that the creep rate is significantly different from those of the local region of TA2 welded joints.

Because the mechanical property distribution of welding joint is locally inhomogeneous, the effects of heat treatment on the mechanical property distribution and matching degree of the Cr-Mo steel welding joint with nickel-based welding material were investigated by DIC method in this research. Then, the hardness tests and microstructure observation were conducted to study the influence of the heat treatment on the distributions of hardness and microstructure. Moreover, the distributions of mechanical properties were correlated with those of microstructures.

1 Experiment

15CrMoR alloy has good mechanical properties and high-temperature creep resistance performance at 550 °C. However, the cold crack and temper brittleness often appear during the welding process for Cr-Mo steel^[22]. Therefore, the mechanical properties of Cr-Mo steel welding joint attract more and more attention^[2,23,24], and the nickel-based welding material is used to achieve better strength. In this research, the pressure vessel metal 15CrMoR steel and ENiCrMo-3 alloy were used as base metal and welding material, respectively. The 15CrMoR

plates with the length of 200 mm, the width of 170 mm, and the thickness of 16 mm were welded by the multi-layer and multi-pass manual arc welding. The welding direction was perpendicular to the rolling direction of 15CrMoR plate. According to the welding standard (GB/T 985.1-2008), the V-shape groove with the groove angle of 35° and the blunt edge of 2 mm was adapted on the welding plate edge for the butt welding. The preheating temperature was 100 °C, while the inter-pass temperature was 100~300 °C. Other welding process parameters are listed in Table 1.

The mechanical properties of the as-received, tempered, and STA-treated nickel-based welding joints were investigated. The tempering heat treatment process was 680 °C/2 h/air cooling, and the STA treatment process was 935 °C/1 h/furnace cooling to 720 °C+720 °C/8 h/furnace cooling to 620 °C+620 °C/8 h.

The as-received, tempered, and STA-treated welding joints were machined, and then the uniaxial tensile specimens with the gauge length of 60 mm, the width of 4 mm, and the thickness of 2 mm were obtained by wire cutting. WFZ is located at the center of uniaxial tensile specimen, as shown in Fig. 1. The 400#~1000# sandpapers were used to polish the specimen surface. Then the parallel section of the specimen was sprayed by speckles, i.e., the specimen was sprayed with a layer of white paint firstly and then with the black paint dots on the white paint surface. The uniaxial tensile tests were conducted on the CTM504-B1 electronically controlled mechanical testing machine, and the test displacement rate was 0.3 mm/min.

During the tensile test, the speckle image on the specimen surface was acquired by the high-definition imaging device, and the GOM non-contact strain measurement system was used to calculate the full-field strain distribution of the welding joint. The resolution of the camera image was 6000×4000 pixels, the facet size used for DIC calculation was 24 pixels, the dot pitch was 12 pixels, the sub-pixels were calculated by the bicubic interpolation, and the maximum interaction deviation was 0.3 pixel.

In order to obtain the hardness distribution on the welding joint, the Lianer HVS-1000 digital microhardness testing device was used. The head pressure was 9.8 N and the load time was 10 s. The hardness was tested at the points at interval of 0.5 mm from the center to the outside of the welding joints. The surface was polished to avoid the influence of roughness on the hardness.

To analyze the influence of heat treatment on metallographic microstructure of the welding joint, the KEYENCE VHX-700F optical microscope (OM) was used to observe the microstructure distribution of the welding joints. After metallographic polishing, BMZ was corroded by nitric acid, and WFZ was corroded by the aqua regia solution (the

Table 1 Welding process parameters and radiographic test results

| Welding method | Joint type | Voltage/V | Current/A | Welding speed/mm·s ⁻¹ | Inspection method | Test standard | Grade |
|--------------------|------------|-----------|-----------|----------------------------------|--------------------------|-----------------|-------|
| Manual arc welding | Butt joint | 20~25 | 100~160 | 1~2 | Radiological examination | NB/T 47013-2015 | I |

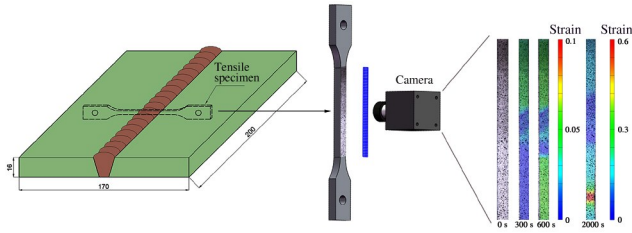


Fig.1 Schematic diagrams of specimen preparation and full-field strain measurement by DIC method

volume ratio of HCl:HNO₃=3:1).

2 Results and Discussion

2.1 Effect of heat treatment on nominal stress-strain curve of nickel-based welding joints

Fig.2 shows the nominal stress-strain curves of the welding joints with the gauge length of 60 mm after different heat treatments, and the nominal mechanical properties can be determined, as listed in Table 2.

The yield stress of the as-received welding joint is the largest, that of the tempered welding joint takes the second place, and that of the STA-treated welding joint is the lowest. The order of ultimate strength of welding joints after different heat treatments is the same as that of the yield stress of

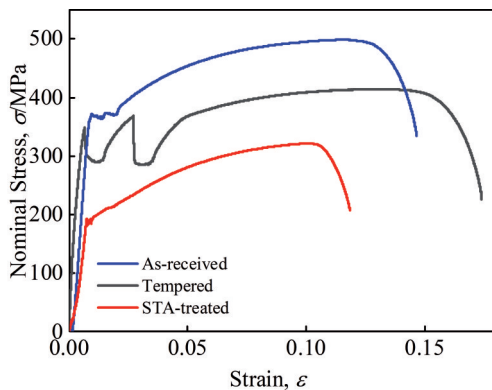


Fig.2 Nominal stress-strain curve of welding joints after different heat treatments

Table 2 Nominal mechanical properties of welding joints after different heat treatments

| Heat treatment | Yield stress/MPa | Ultimate strength/MPa | Elongation/% |
|----------------|------------------|-----------------------|--------------|
| As-received | 367 | 507 | 15 |
| Tempering | 290 | 412 | 17 |
| STA | 200 | 324 | 12 |

welding joints. The elongation of the tempered welding joint is the longest, that of the as-received welding joint takes the second place, and that of the STA-treated welding joint is the shortest. It is interesting that the as-received and the tempered welding joints show the secondary yielding phenomenon, i.e., there is a sudden decrease in stress after the primary yielding, and then the secondary hardening and yielding phenomena occur in the as-received and the tempered welding joints. This result can be explained by the following reasons. The strength of the 15CrMoR base metal is lower than that of the ENiCrMo-3 nickel-based welding material, and there are two BMZs on both sides of WFZ. Then the two BMZs yield in turn, so the secondary yielding phenomenon can be observed from the nominal stress-strain curve.

2.2 Effect of heat treatment on local strain field distribution and stress-strain map of nickel-based welding joints

Although the nominal stress-strain curves in Fig. 2 can indicate the comprehensive mechanical properties of WFZ, HAZ, and BMZ of welding joints, the related strength parameters are restricted by the weakest section. Therefore, the nominal stress-strain curves cannot be used to investigate the influence of heat treatment on the mechanical property distribution at different zones of welding joints. In order to obtain the local stress-strain curves, DIC method was used to obtain the full-field strain distribution in WFZ, HAZ, and BMZ for welding joints after different heat treatments. Fig.3 shows the strain distribution curves of the welding joints at different loading displacements by DIC method.

As shown in Fig.3a, the strain distributions in WFZ of the as-received welding joint are significantly inhomogeneous, which is related to the inhomogeneity of the dendrite structure

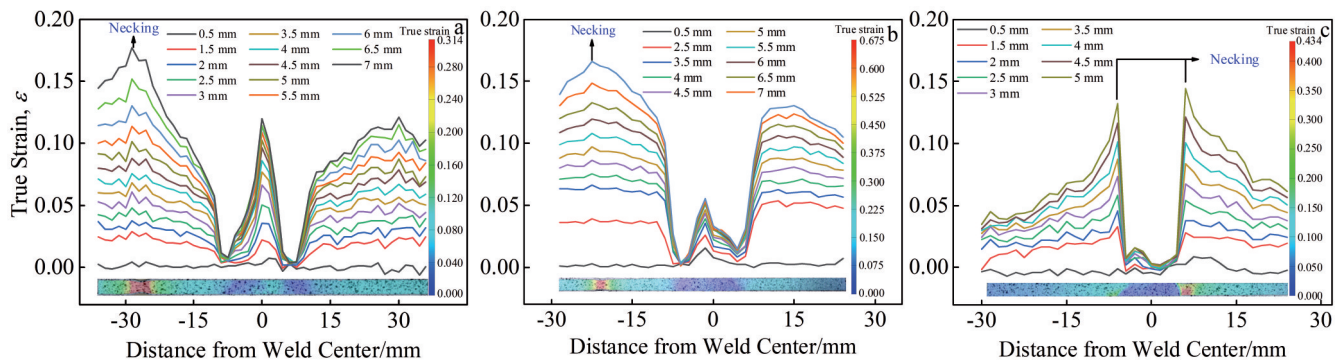


Fig.3 Quantitative strain distribution curves of as-received (a), tempered (b), and STA-treated (c) welding joints at different loading displacements by DIC method

and the element concentration distribution in WFZ. The necking phenomenon firstly occurs in BMZ, because the strength of the base metal is lower than that of the nickel-based welding material. As shown in Fig. 3b, the strain homogeneity in WFZ of tempered welding joints is improved, the strain in BMZ is significantly higher than that in WFZ, and the necking phenomenon still occurs in BMZ. As shown in Fig. 3c, the strain homogeneity in WFZ of STA-treated welding joint is further improved, but the necking area changes to the boundary between WFZ and BMZ. It is worth noting that there is a strain gradient transition region between BMZ and WFZ for the as-received and tempered welding joints, as shown in Fig. 3a and 3b, respectively. However, for STA-treated welding joint, the strain gradient transition region disappears and the strain variation is abrupt. For the as-received welding joint, the appearance of the strain gradient transition region is caused by the deformation compatibility and element diffusion during the welding process. For the tempered welding joint, the variation of microstructure is restricted, and then the strain gradient transition region remains. However, for the STA-treated welding joint, the microstructures of both BMZ and WFZ are changed greatly. Thus, the strain gradient transition region disappears.

Based on the results, a three-dimensional full-field true stress-true strain map can be constructed. The local stress is related to the load and the cross-sectional area^[25], which can be expressed as follows:

$$\sigma^i = F/A^i \quad (1)$$

$$A^i = A_0^i \exp(-\varepsilon^i) \quad (2)$$

where σ^i is the local stress, F is the instantaneous load, A^i is the local cross-sectional area, A_0^i is the initial cross-sectional area, and ε^i is the local strain. The abovementioned theory is based on the assumption that the metal volume does not change during tensile tests. But after necking, the stress triaxiality increases rapidly, and the cross-section is distorted. Therefore, the hypothesis of volume invariance is invalid^[26-29] and the local stress formula cannot be used to describe the stress-strain relationship after necking. Through the local stress obtained by the load sensor and the local strain obtained by DIC method, the full-field true stress-true strain map of the welding joint can be constructed, as shown in Fig. 4. WFZ is the area with the distance of ± 8 mm from the weld center, BMZ includes the area with the distance beyond ± 12 mm from the weld center, and HAZ is the middle area between WFZ and BMZ.

It can be seen from the full-field true stress-true strain map of the as-received welding joint (Fig. 4a) that there is a significant difference in the true stress-true strain curve between WFZ and BMZ. The true stress-true strain curve at the fracture area of BMZ is complete, but that of WFZ only contains a certain range of strain, because there is no necking or fracture phenomenon in WFZ during the tensile process and the true stress-true strain curve of WFZ is incomplete. For the as-received welding joint, the true stress-true strain curve

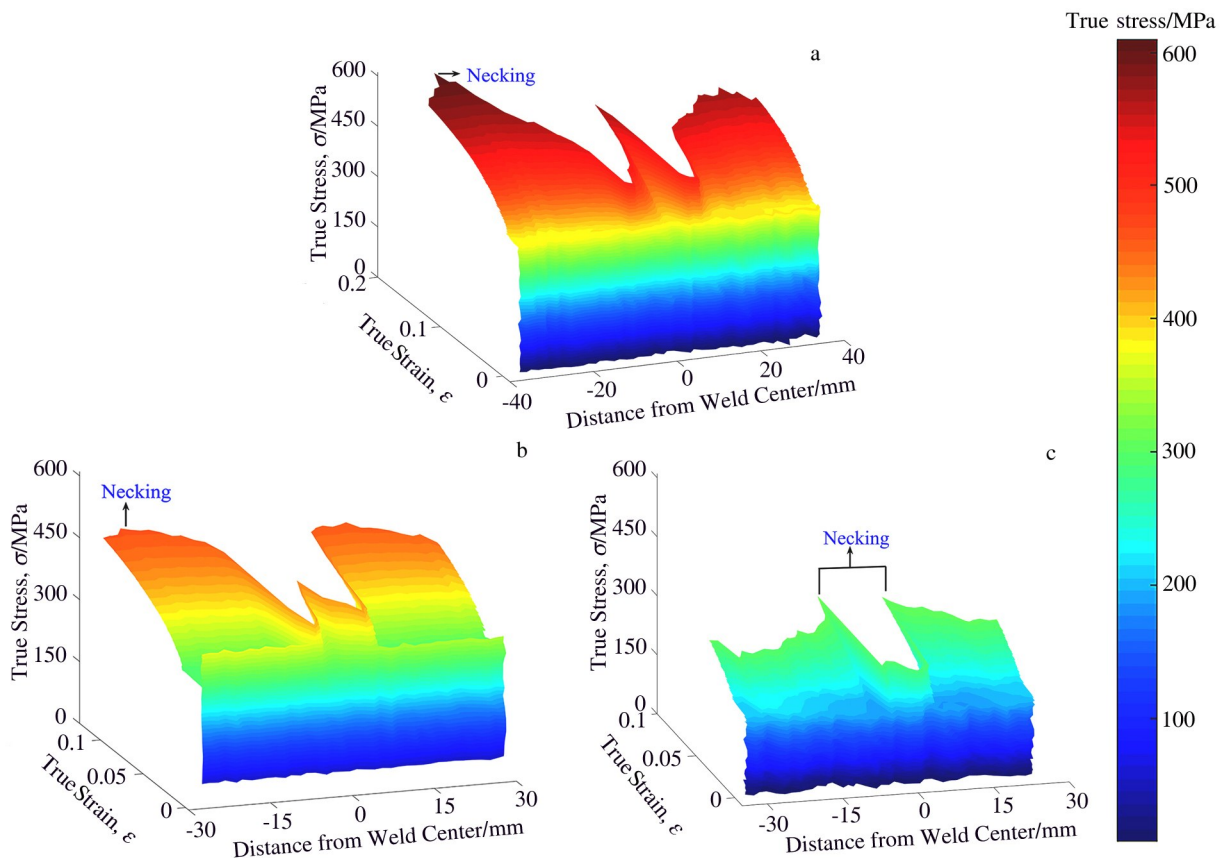


Fig.4 True stress-true strain maps of as-received (a), tempered (b), and STA-treated (c) welding joints

of WFZ is inhomogeneous; for the tempered welding joint, the homogeneity of WFZ is improved and the strengths of WFZ and BMZ are slightly reduced. After STA treatment, the homogeneity of the true stress-true strain curve of WFZ is further improved, but the strength of WFZ and BMZ is significantly reduced. The failure position is transferred from BMZ to the boundary between WFZ and BMZ.

Based on the full-field true stress-true strain maps, the yield stress distributions of different zones are shown in Fig. 5. It can be seen that the yield stress of WFZ is higher than that of BMZ, and the transition occurs on HAZ. It is worth noting that there are obvious fluctuations of the yield stress of WFZ, and the yield stress of WFZ in the as-received welding joint

has the fluctuation range of about 67 MPa. The tempering treatment alleviates the structural inhomogeneity of WFZ, and thereby the fluctuation range of yield stress is reduced to 45 MPa. STA treatment further improves the microstructure homogeneity of WFZ, and the fluctuation range of yield stress is reduced to about 40 MPa.

The yield stress difference between WFZ and BMZ is an important mismatching parameter for the welding joints, which is relatively small of about 45 MPa for both the as-received and tempered welding joints. However, after STA treatment, the yield stress difference between WFZ and BMZ significantly increases to about 80 MPa. Therefore, after STA treatment, the mismatching degree of yield stress between BMZ and WFZ is increased, causing the transference of the failure position to the connection boundary of BMZ and WFZ, and the fracture elongation is reduced.

2.3 Effect of heat treatment on hardness distribution of nickel-based welding joints

The hardness distribution can be easily obtained by the hardness tests^[30]. Fig. 6 shows the hardness distributions and the yield stress distributions of different welding joints. It is worth noting that there is a close relationship between yield stress and hardness for all welding joints. For the as-received welding joint (Fig.6a), the hardness fluctuates greatly in WFZ, and the average hardness of WFZ is higher than that of BMZ by about 980 MPa. After tempering treatment, the homogeneity of the hardness distribution in WFZ is improved, and the hardness difference between WFZ and BMZ is reduced to about 539 MPa. After STA treatment, the hardness distribution is more uniform, but the hardness difference

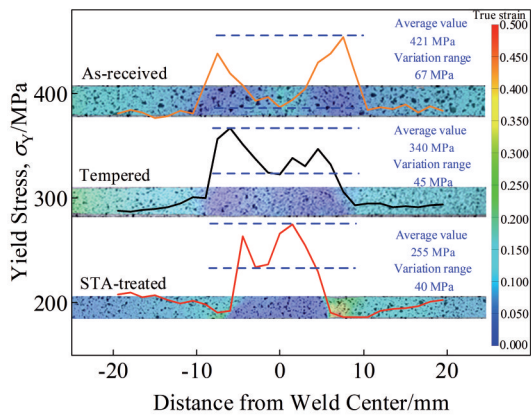


Fig.5 Yield stress distribution curves of welding joints after different heat treatments

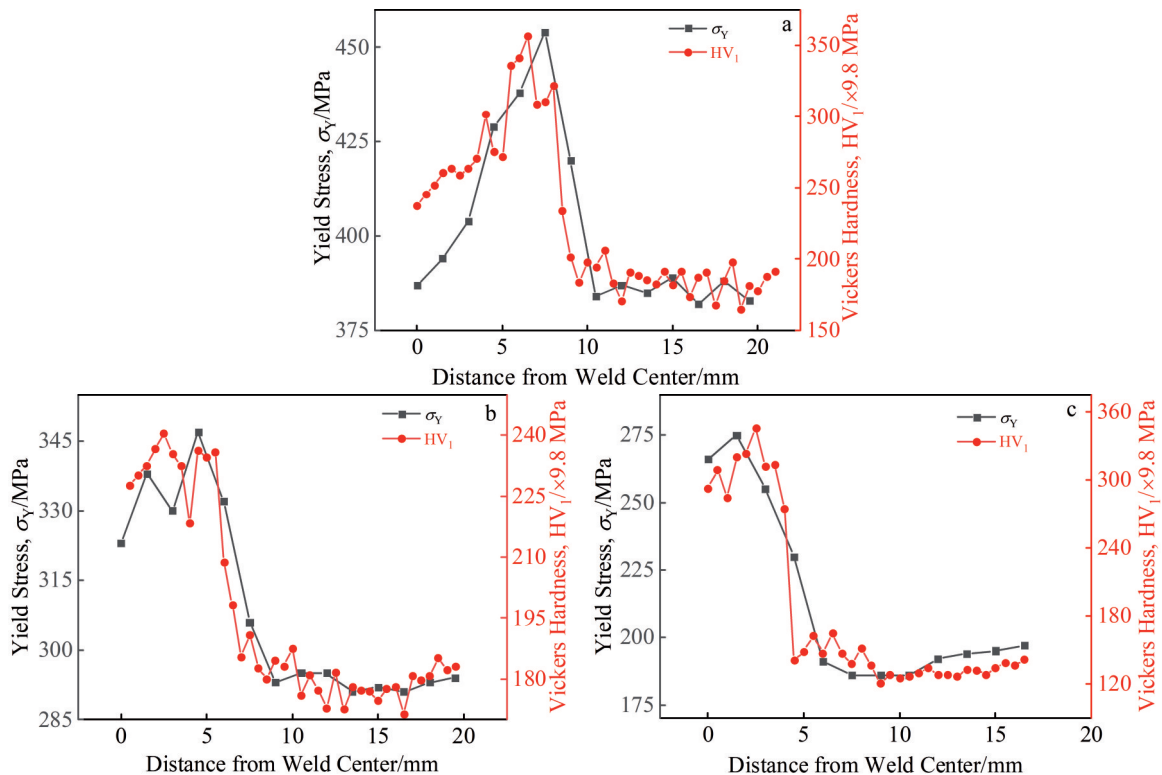


Fig.6 Hardness and yield stress distributions of as-received (a), tempered (b), and STA-treated (c) welding joints

between WFZ and BMZ is significantly increased to about 1960 MPa, indicating that the mismatching degree of hardness between WFZ and BMZ is increased.

Since there is a close correlation between the hardness and the yield stress, Cahoon et al.^[31] proposed an empirical equation to predict the yield stress by the hardness and strain hardening index, as expressed in Eq.(3), as follows:

$$\sigma_Y = (H/A)B^n \quad (3)$$

where A and B are the correlating parameters obtained by data fitting; σ_Y is the yield stress; H is the hardness; n is the strain-hardening exponent.

Pavlina et al.^[32] used the least-squares linear regression to obtain the correlation equation of hardness and yield stress for the non-austenitic hypoeutectoid steel, as expressed by Eq.(4), as follows:

$$\sigma_Y = CH_V + D \quad (4)$$

where C and D are parameters obtained by data fitting; H_V is the hardness. According to Fig.6, the hardness and yield stress of nickel-based welding joints are linearly correlated, and therefore the correlated equations between hardness and yield stress of the as-received, tempered, and STA-treated welding joints can be fitted by Eq.(5~7), respectively:

$$\sigma_Y = 0.36H_V + 320.61 \quad (5)$$

$$\sigma_Y = 0.81H_V + 150.10 \quad (6)$$

$$\sigma_Y = 0.40H_V + 140.71 \quad (7)$$

The predicted yield stress is compared with the experimental one obtained by DIC experiments, as shown in Fig.7. The error certainly exists in the predicted yield stress of WFZ of as-received welding joint due to the large fluctuations in hardness and yield stress, and the predicted yield stresses of other regions are in good agreement with DIC experimental data. Therefore, the hardness distribution can indirectly represent the tensile yield stress distribution of the welding joints.

2.4 Effect of heat treatment on metallographic microstructure of nickel-based welding joints

Fig.8 shows the metallographic microstructures of WFZ of welding joints after different heat treatments. It can be seen from Fig. 8a that the WFZ microstructure of as-received welding joint is mainly composed of dendrites. The dendrite wall spacing is discrete in WFZ of as-received welding joint,

and the equiaxed dendrites coexist with the coarse columnar dendritic structure. The equiaxed dendrites near the weld bead are refined, resulting in higher strength near the weld bead. The inhomogeneity of the microstructure at the weld seam leads to the inhomogeneity of the mechanical property distribution of the as-received welding joint. Fig.8b shows the metallographic microstructure of WFZ in welding joint after tempering treatment. The inhomogeneous dendrites of the as-received welding joint are transformed into the tempered sorbite^[33], while the dispersion of carbides is improved. Therefore, after tempering treatment, the homogeneity of mechanical property distribution of WFZ in welding joint is improved, while the strength of WFZ is reduced. Fig.8c shows the metallographic microstructure of WFZ in welding joint after STA treatment, presenting the columnar dendritic structure. Since the grain size is uniform, the uniformity of the metallographic structure in WFZ is significantly improved. After STA treatment, WFZ shows the uniform distribution of mechanical property, and the strength is improved.

Fig.9 shows the metallographic microstructures of BMZ of welding joints after different heat treatments. According to Fig. 9a, the BMZ microstructure shows the dual-phase structure of massive ferrite and pearlite in the as-received welding joint, and the volume fraction of ferrite and pearlite is similar. As shown in Fig.9b, after tempering treatment, the percentage of pearlite in BMZ is reduced. More carbon is dissolved into the pearlite during the tempering process. These microstructure changes cause the decrease in hardness and strength and the increase in toughness and plasticity of BMZ in welding joint after tempering treatment. Fig.9c shows the BMZ microstructure in welding joint after STA treatment, which is full of ferrite without pearlite. The crystal grains become coarse, which causes the decrease in dispersible deformable grains. Then, the plastic deformation becomes inhomogeneous and the cracks are prone to occur. Therefore, both strength and ductility of BMZ are reduced after STA treatment.

STA treatment increases the mismatching degrees of both microstructure and mechanical property, and the failure appears at the mismatching connection position between BMZ and WFZ. After tempering treatment, the microstructure of BMZ is not damaged, the toughness is improved, and the

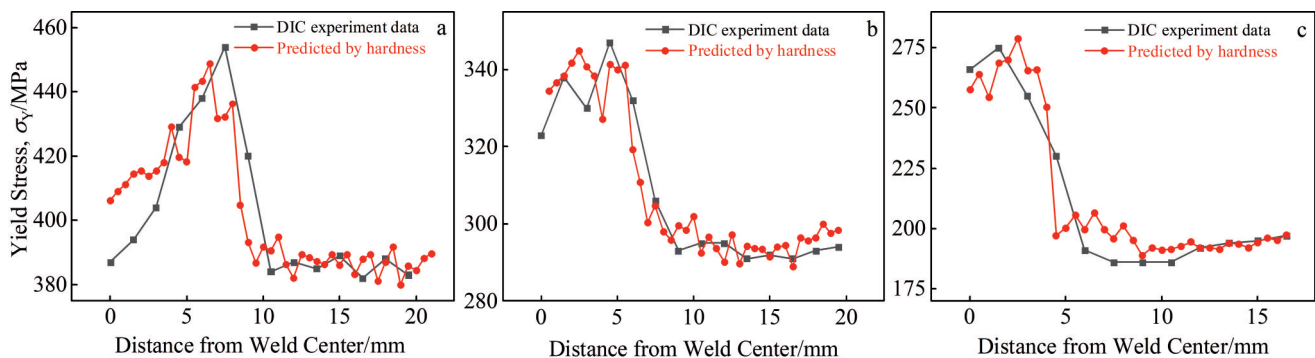


Fig.7 Predicted and experimental yield stress distributions of as-received (a), tempered (b), and STA-treated (c) welding joints



Fig.8 Metallographic microstructures of WFZ in as-received (a), tempered (b), and STA-treated (c) welding joints

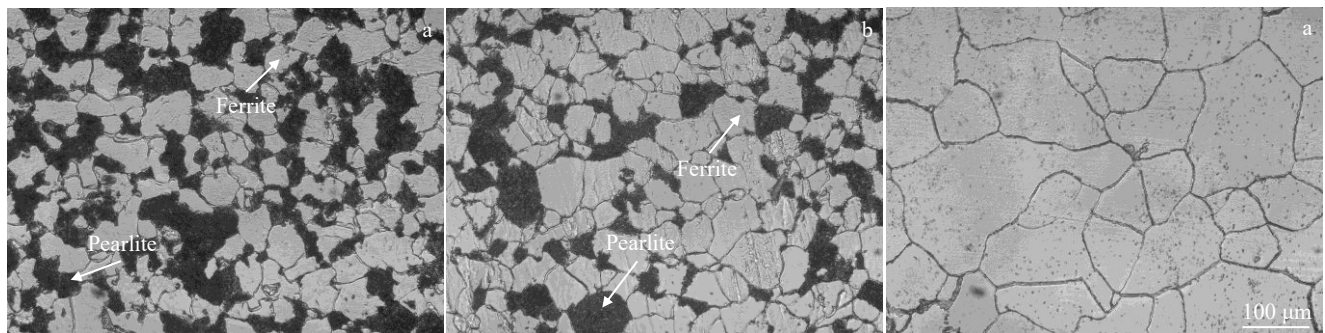


Fig.9 Metallographic microstructures of BMZ in as-received (a), tempered (b), and STA-treated (c) welding joints

uniformity of the microstructure in WFZ is improved. Therefore, the matching degree of the mechanical properties between BMZ and WFZ is improved. In conclusion, the tempering treatment can achieve the optimal amelioration between BMZ and WFZ. STA treatment can only improve WFZ, whereas BMZ structure and mechanical properties are worse after STA treatment.

3 Conclusions

1) Based on the digital image correlation analyses and hardness tests, the distributions of strain, stress-strain curve, yield stress, and hardness are inhomogeneous in welding fusion zone (WFZ) of the as-received welding joint, and the fracture originates from the base metal zone (BMZ). The tempering treatment improves the uniformity of the mechanical property of WFZ without changing the failure location. The solution treatment and aging (STA) treatment can further improve the uniformity of the mechanical property of WFZ in welding joint, but it significantly degenerates the mechanical properties of BMZ, therefore increasing the mismatching degree of mechanical properties between BMZ and WFZ. The fracture position after STA treatment transfers to the boundary between BMZ and WFZ.

2) The dendrite wall spacing is discrete in WFZ of as-received welding joint, and the equiaxed dendrites coexist with the coarse columnar dendritic structure, resulting in the inhomogeneous distributions of both microstructure and mechanical properties in WFZ of as-received welding joint. The tempering treatment changes the dendrites into the

dispersed sorbites, which improves the uniformity of both microstructure and mechanical properties of WFZ of tempered welding joint, and the matching degree between BMZ and WFZ is improved. Although STA treatment can uniformize the microstructure and mechanical properties of WFZ, the grains are coarsened and the microstructure is damaged in BMZ, resulting in the degradation of the matching degree between BMZ and WFZ.

3) The tempering treatment can achieve the optimal amelioration between BMZ and WFZ. STA treatment can only improve WFZ, whereas BMZ structure and mechanical properties are worse after STA treatment.

References

- 1 Anbarasan N, Jerome S, Manikandan S G K. *Materials Science and Engineering A*[J], 2020, 773: 138 874
- 2 Kumar S, Yadav V K, Sharma S K et al. *International Journal of Pressure Vessels and Piping*[J], 2021, 193: 104 443
- 3 Guo L L, Zheng H L, Liu S H et al. *Rare Metal Materials and Engineering*[J], 2016, 45(9): 2219
- 4 Lu Q B, Zhong S J, Li S G et al. *Rare Metal Materials and Engineering*[J], 2019, 48(8): 2418
- 5 Mittal R, Sidhu B S. *Journal of Materials Processing Technology* [J], 2015, 220: 76
- 6 Kumar S, Singh P K, Karn K N et al. *Fatigue and Fracture of Engineering Materials and Structures*[J], 2017, 40(2): 190
- 7 Awale D D, Ballal A R, Thawre M M et al. *Journal of Nuclear Materials*[J], 2020, 532: 152 048

- 8 Wang G Q, Chen M S, Li H B et al. *Journal of Materials Science and Technology*[J], 2021, 77: 47
- 9 Wang G Q, Li H B, Chen M S et al. *Materials Characterization* [J], 2021, 176: 111 130
- 10 Qi X Q, Liu Z H, Li X. *Journal of Physics: Conference Series* [J], 2021, 1865(3): 32 023
- 11 Xu F J, Lv Y H, Liu Y X et al. *Physics Procedia*[J], 2013, 50: 48
- 12 Wan Y, Jiang W C, Wei W et al. *Materials Science and Engineering A*[J], 2021, 822: 141 640
- 13 Peters W H, Ranson W F. *Optical Engineering*[J], 1982, 21(3): 213 427
- 14 Yamaguchi I. *Journal of Physics E: Scientific Instruments*[J], 1981, 14(11): 1270
- 15 McCormick N, Lord J. *Materials Today*[J], 2010, 13(12): 52
- 16 Pan B, Qian K M, Xie H M et al. *Measurement Science and Technology*[J], 2009, 20(6): 152
- 17 Li G Y, Xu F X, Sun G Y et al. *The International Journal of Advanced Manufacturing Technology*[J], 2014, 74(5): 893
- 18 Xie X F, Li J W, Jiang W C et al. *Materials Science and Engineering A*[J], 2020, 786: 139 426
- 19 Ren X Y, Xu X Y, Jiang C X et al. *Optics and Lasers in Engineering*[J], 2020, 124: 105 839
- 20 Hu Dianyin, Yang Qian, Liu Huawei et al. *Rare Metal Materials and Engineering*[J], 2017, 46(11): 3405 (in Chinese)
- 21 Sun P Y, Zhu Z K, Su C Y et al. *Optics and Lasers in Engineering*[J], 2019, 115: 161
- 22 Ahmed S R, Agarwal L A, Daniel B S S. *Materials Today: Proceedings*[J], 2015, 2(4-5): 1059
- 23 Mittal R, Gupta A, Pratap K et al. *Materials Today: Proceedings* [J], 2020, 26(2): 316
- 24 Zhao S X, Wang M J, Kou S Z et al. *Fusion Engineering and Design*[J], 2020, 158: 111 699
- 25 Peng Y, Wu C, Gan J L et al. *Construction and Building Materials*[J], 2018, 171: 485
- 26 Yun L. *AMP Journal of Technology*[J], 1996, 5(1): 37
- 27 Jia L J, Kuwamura H. *Journal of Structural Engineering*[J], 2014, 140(5): 4 013 115
- 28 Jia L J, Ge H B, Shinohara K et al. *Journal of Bridge Engineering*[J], 2016, 21(5): 4 016 008
- 29 Jia L J, Ikai T, Shinohara K et al. *Construction and Building Materials*[J], 2016, 112: 69
- 30 Luo Hailong, Zhang Min, Mu Erlong et al. *Transactions of the China Welding Institution*[J], 2019, 40(1): 141 (in Chinese)
- 31 Cahoon J R, Broughton W H, Kutzak A R. *Metallurgical Transactions*[J], 1971, 2(7): 1979
- 32 Pavlina E J, Van Tyne C J. *Journal of Materials Engineering and Performance*[J], 2008, 17(6): 888
- 33 Jiang Z Z, Ren L T, Huang J H et al. *Fusion Engineering and Design*[J], 2010, 85(10-12): 1903

热处理对Cr-Mo钢母材-镍基焊材焊接接头力学性能分布及匹配度的影响

彭 剑, 屠 懿, 薛智超, 缪新婷, 刘雪东

(常州大学 机械与轨道交通学院, 江苏 常州 213164)

摘 要: 依托数字图像相关技术在表征焊接接头局部力学性能方面的优势, 对比研究了原始态、回火态和固溶时效态 15CrMoR 母材与镍基焊材组成的焊接接头的力学参数、硬度和显微组织。回火处理使焊接熔合区的枝晶组织转变为分散的回火索氏体, 提高了力学性能的均匀性, 改善了母材区与焊接熔合区力学性能的匹配程度。固溶时效处理促使焊接熔合区的枝晶组织转变为均匀的柱状枝晶组织, 同时母材区的珠光体消失、晶粒粗化, 导致强度下降, 引起焊接熔合区与母材区的不匹配度增大。因此, 合适的热处理要求平衡母材区和焊缝区对组织的需要, 以获得具有优良综合力学性能的焊接接头。

关键词: 镍基合金焊接接头; 热处理; 数字图像相关技术; 力学性能分布

作者简介: 彭 剑, 男, 1987年生, 博士, 副教授, 常州大学机械与轨道交通学院, 江苏 常州 213164, E-mail: jpeng@cczu.edu.cn